

# A statistical veto method employing an amplitude consistency check

S Hild, P Ajith, M Hewitson, H Grote and J R Smith

Max-Planck-Institut für Gravitationsphysik (Albert-Einstein-Institut) and Leibniz Universität Hannover, Callinstr. 38, D-30167 Hannover, Germany

E-mail: [stefan.hild@aei.mpg.de](mailto:stefan.hild@aei.mpg.de)

Received 18 January 2007, in final form 22 June 2007

Published 17 July 2007

Online at [stacks.iop.org/CQG/24/3783](http://stacks.iop.org/CQG/24/3783)

## Abstract

Statistical veto methods are commonly used to reduce the list of candidate gravitational wave (GW) events which are detected as transient (burst) signals in the main output of GW detectors. If a burst event in the GW channel is coincident with an event in a veto channel (where the veto channel does not contain any GW signal), it is possible to veto the event from the GW channel with a low ‘false-veto’ rate. Unfortunately, many promising veto channels are interferometer channels which can, at some level, contain traces of any detected GW signal. In this case, the application of a ‘standard statistical veto’ could have a high false-veto rate. We will present an extension to the standard statistical veto method that includes an ‘amplitude consistency check’. This method allows the application of statistical vetoes derived from interferometer channels containing GW information with a low false-veto rate. By applying a statistical veto with an amplitude consistency check to data from the GEO 600 detector, veto efficiencies between 5 and 20%, together with a use-percentage of up to 80%, were obtained. The robustness of this veto method was also confirmed by hardware injections. The burst triggers were generated using the mHACR detection algorithm.

PACS numbers: 95.55.Ym, 04.80.Nn

(Some figures in this article are in colour only in the electronic version)

## 1. Introduction

One of the most exciting classes of gravitational wave (GW) signatures that may be detected by the current array of ground-based laser interferometric GW detectors [1–4] is unmodelled transient (burst) signals arising from short-lived, violent astronomical events. The search for such signals typically focuses on time scales of the order of a few (or few tens of) milliseconds.

Due to their extremely complicated nature, GW detectors are themselves usually potent sources of transient signals. A subset of these signals arising from many different subsystems within the detectors can (and do) couple to the main detector output, and hence appear as false GW triggers in any search effort looking for unknown signals. While a great amount of effort is afforded in the reduction of these instrumental and environmental glitches and/or their coupling to the main detector output (also termed the  $H$  channel when properly calibrated), there is still a residual amount of non-GW transients that remains.

Once the glitch population of a particular subsystem, and its coupling to the GW channel, is physically reduced to a minimum, the residual must be identified and characterized so as to exclude those glitches from the search for GWs. The rate of glitches in the GW channel ultimately sets a limit on the confidence with which a particular trigger can be identified as a GW. It is therefore important to try and reduce the number of glitches in the GW channel that are to be considered in a search for GWs. This is traditionally done by *vetoing* those events detected in  $H$  using knowledge of events detected in auxiliary channels. Once an auxiliary channel has been identified as being a source of transient events which couple to  $H$ , it is termed a veto channel and is then studied and used to reduce the event list of  $H$ .

The application of the veto is done by identifying those events in the auxiliary channel which are, in some way, coincident with events detected in  $H$ . Detected glitches are typically characterized by a few parameters (time of occurrence, amplitude, central frequency, etc), such that saying that two events are coincident can be as simple as saying that they occur at the same time (within some error window) or as complicated as saying that many of the characteristics of the glitches are (within some defined windows) the same. When a parameterization of glitch events is used to compare events between data streams, we refer to the resulting veto as a *statistical* veto since its performance is based on the statistical properties of the distributions of glitches in the two data streams and does not rely on any knowledge of the physical coupling mechanisms involved. Examples of the application of statistical veto methods to GW detector data can be found in [9–11]. Another class of veto method which relies on detailed knowledge of the coupling mechanism involved in transporting glitches from a particular subsystem to the  $H$  channel, and also uses the full data streams, is not discussed here, but an example is given in [5]. There are also interferometer channels which, by definition, contain negligible GW information but can nevertheless remain highly correlated to the main GW channel. These ‘null-stream’ channels can also be used as effective veto channels (see [6–8] for examples). In addition to these single-detector veto methods, there is active research in the use of multiple detector outputs as a means of vetoing candidate events (see, for example, [12–16]).

The application of vetoes can, of course, lead to *false vetoes*, that is, events in the auxiliary channel which are only accidentally coincident with events in the  $H$  channel but which are nevertheless used to veto an event in  $H$ . Requiring that more glitch characteristics be ‘similar’ when performing the coincident test can reduce the false-veto rate (usually at the cost of a reduced veto efficiency). The usefulness of a particular veto channel can be characterized according to the number of  $H$  events it can veto (veto efficiency) for a given number of false vetoes (false/accidental-veto rate). In addition, vetoes are characterized by the amount of data they remove from any particular search (dead time), and also by how many glitches from the auxiliary channel can be used to veto an event in the main gravitational wave channel (use-percentage).

This paper investigates many aspects of the identification, characterization and use of veto channels for data recorded from GEO 600, in particular for the case when the veto channel in question can contain GW information. Section 2 describes the burst detection algorithm used in these studies and discusses the errors associated with each parameter of the detected events, at least for a simple case. Section 3 goes on to discuss the *standard* statistical veto

and shows an example application (with single and multiple coincidence windows) to data from GEO 600. Section 4 shows a possible extension to the standard statistical veto method for the case where the auxiliary channel can contain traces of GW signals, i.e., the sensitivity of the auxiliary channel is less than the main GW channel but is non-negligible. Section 5 shows the application of the extended standard statistical veto method to GEO 600 data.

## 2. Production of burst event triggers

The *hierarchical algorithm for curves and ridges* (HACR) [17, 18] is a transient-detection algorithm based on a time–frequency detection method. This algorithm was first implemented as part of the GEO++ software environment and was subsequently modified over time to form the *modified HACR* (mHACR) algorithm. The burst triggers studied throughout this paper were generated using mHACR. A brief description of the mHACR algorithm is given below.

### 2.1. Detection algorithm

The discretely sampled time-series data  $h_j$  is divided into  $n$  short segments of length  $L$  and the discrete Fourier transform (DFT) of each segment is computed after multiplying the time-series data with a suitable window function  $w_j$ :

$$\tilde{H}_{kl} = \sum_{j=l(L-O)}^{l(L-O)+L-1} h_j w_j \exp(i2\pi jk/L), \quad k = 0, \dots, L/2, \quad l = 0, \dots, n-1. \quad (1)$$

The length,  $L$ , of the segment is chosen according to the time scale of the burst signals that we are trying to detect (expected to range from a few milliseconds to a few tens of milliseconds). Typically,  $L$  is chosen to be 32 ms long, and a Hann window is used to avoid edge effects. Because of the window function, only the data at the centre of each segment make a significant contribution to the DFT. We therefore allow sufficient (typically  $\geq 75\%$ ) overlap,  $O$ , between consecutive segments to make sure that each sample is ‘properly’ represented in the time–frequency map.

Often we are interested only in detecting non-stationarities appearing within some specific frequency band (say, where the detector is most sensitive). So, only frequency bins above a lower cutoff frequency,  $f_{\text{low}}$ , and below an upper cutoff frequency,  $f_{\text{upp}}$ , are retained in the constructed time–frequency map. These cutoff frequencies can be specified as input parameters to mHACR.

The time–frequency representation of the data that we use is called a *spectrogram*:

$$\rho_{kl} = 2A|\tilde{H}_{kl}|^2, \quad (2)$$

where  $A$  is a normalization factor, chosen in such a way that  $\rho_{kl}$  has units of power spectral density, i.e.,  $A = (f_s \sum_j w_j^2)^{-1}$ , and  $f_s$  is the sampling frequency of the data. One can associate a certain Fourier frequency,  $f_k$ , and time,  $t_l$ , with each time–frequency pixel,  $\rho_{kl}$ , such that

$$f_k = kf_s/L, \quad t_l = [l(L-O) + L/2]f_s^{-1}. \quad (3)$$

We will use these quantities while estimating the parameters of the burst triggers.

After constructing the time–frequency matrix,  $\rho$ , we want to identify time–frequency pixels,  $\rho_{kl}$ , which are statistically different from the background noise. We first estimate the mean,  $\mu_k$ , and standard deviation,  $\sigma_k$ , of each row (frequency bin) of the matrix  $\rho$ . In each frequency bin,  $\Omega$  fraction of time–frequency pixels having the highest values of  $\rho_{kl}$  is excluded from this estimation. The *fraction of outliers*,  $\Omega$ , is specified as an input parameter

**Table 1.** Input parameters required by mHACR and the values used for the analysis described in section 2.3.

Parameter	Description	Value used
$f_s$ (Hz)	Sampling frequency of the data	16 384
$L$	Number of samples in one segment	512
$O$	Number of overlapping samples	384
$f_{\text{low}}$ (Hz)	Low frequency cutoff	128
$f_{\text{high}}$ (Hz)	High frequency cutoff	3008
$\Omega$	Fraction of outliers to be excluded in the parameter estimation of the noise	0.1
$T_{\text{low}}$	Lower threshold on pixel significance	5
$T_{\text{upp}}$	Upper threshold on pixel significance	20

to mHACR, and, ideally, should be chosen in such a way that the non-Gaussian tails of the background noise distribution are excluded from the estimation of its mean and variance. We then calculate the *significance*,  $s_{kl}$ , of each pixel,  $\rho_{kl}$ , as

$$s_{kl} = \frac{\rho_{kl} - \mu_k}{\sigma_k}. \quad (4)$$

We assign the following ‘colours’ to each time–frequency pixel, according to the following criteria:

$$\text{colour}(\rho_{kl}) = \begin{cases} \text{black,} & \text{if } s_{kl} \geq T_{\text{upp}} \\ \text{grey,} & \text{if } T_{\text{upp}} > s_{kl} \geq T_{\text{low}} \\ \text{white,} & \text{if } s_{kl} < T_{\text{low}}, \end{cases}$$

where  $T_{\text{upp}}$  and  $T_{\text{low}}$  are the upper and lower thresholds chosen for a particular analysis. Double threshold detection methods are more robust than single threshold methods and are commonly used in satellite imaging, astronomy, particle physics, etc (see, for example, [19, 20]). The neighbouring black and grey pixels are clustered together, and, if a cluster contains at least two pixels, of which at least one is black, then it is identified as a burst *event*. Once the burst events are identified, mHACR proceeds to parameterize the events in terms of a few parameters. The parameter estimation is described below.

The input parameters required by mHACR and the values used for the analysis described in section 2.3 are summarized in table 1.

## 2.2. Parameter estimation

The *total power*,  $P_{\text{tot}}$ , associated with a burst event is the total signal power in all the (black and grey) pixels belonging to a burst event. It should be noted that, because of the overlaps between consecutive data segments, the time–frequency pixels are also overlapping in time. This redundancy in the power distribution among the pixels is taken into account when we estimate the total power by summing the signal power in pixels. We estimate the total power as

$$P_{\text{tot}} = \sum_{k,l} S_{kl} / r, \quad (5)$$

where  $r = L/(L - O)$  is the *redundancy factor* due to the overlapping segments, and the signal power is estimated by subtracting the mean noise power in each frequency bin from  $\rho_{kl}$ , i.e.,  $S_{kl} = \rho_{kl} - \mu_k$ . Throughout this section, the indices range over all the black and grey

pixels belonging to a particular event. mHACR also estimates the *peak power* of the burst event as

$$P_{\text{peak}} = \max(S_{kl}). \quad (6)$$

The estimation of the *central frequency*,  $f_0$ , and *central time*,  $t_0$ , is analogous to the calculation of the centre-of-mass of an extended body. Here, the *signal power*,  $S_{kl}$ , in each time–frequency pixel serves as the ‘mass’ term and the time/frequency associated with each pixel serves as the ‘position’ term. That is,

$$f_0 = \sum_{k,l} S_{kl} f_k / \sum_{k,l} S_{kl}, \quad t_0 = \sum_{k,l} S_{kl} t_l / \sum_{k,l} S_{kl}. \quad (7)$$

The *signal-to-noise ratio* (snr),  $\rho$ , is defined in a similar way to the total power:

$$\rho^2 = \sum_{k,l} \frac{S_{kl}}{\mu_k} / r. \quad (8)$$

Finally, the *duration*,  $d$ , and *bandwidth*,  $b$ , of the burst event can be estimated from the extent of the burst event in the time/frequency plane as

$$d = \max(t_l) - \min(t_l), \quad b = \max(f_k) - \min(f_k). \quad (9)$$

### 2.3. Quality of the parameter estimation

In this section, we demonstrate the accuracy of the parameter estimation by doing software injections into Gaussian white noise and comparing the parameters of the injected waveforms with those estimated by mHACR. The injected waveforms are sine-Gaussians of the form

$$h(t) = h_{\text{rss}} \left( \frac{2f_{\text{cen}}^2}{\pi} \right)^{1/4} \sin[2\pi f_{\text{cen}}(t - t_{\text{cen}})] \exp \left[ \frac{-(t - t_{\text{cen}})^2}{\tau^2} \right], \quad (10)$$

where  $f_{\text{cen}}$  is the central frequency of the waveforms and  $t_{\text{cen}}$  is the time corresponding to the peak amplitude. We set the envelope width as  $\tau = 2/f_{\text{cen}}$ . The corresponding quality factor is  $Q \equiv \sqrt{2}\pi f_{\text{cen}}\tau = 8.9$ . The quantity  $h_{\text{rss}}$  is the root-sum-squared (RSS) amplitude given by

$$\left[ \int_{-\infty}^{\infty} h^2(t) dt \right]^{1/2} = h_{\text{rss}}. \quad (11)$$

Nine different values of  $h_{\text{rss}}$  are used for the injections such that the snr of the injections ranges from  $\simeq 5$  to  $\simeq 300$ , and the central frequency is randomly chosen from the interval (432, 3008) Hz. Since the injections are done with nine different values of  $h_{\text{rss}}$ , we expect the errors in the estimation of each parameter to fall into a multivariate normal distribution of nine dimensions. The sample mean and standard deviation of each of the nine populations are estimated separately. We convert the errors into standard normal variables by subtracting the sample mean from each sample and by normalizing by the standard deviation. Distributions of the errors (after subtracting the mean and normalizing by the standard deviation) are plotted in figure 1, along with the probability density of a normal distribution with mean 0 and variance 1. The figure shows the error distributions of three parameters—the estimated central frequency  $f_0$ , central time  $t_0$  and the RSS amplitude  $a = \sqrt{P_{\text{tot}}}$ . The standard deviation of the errors in the estimation of these parameters are plotted as a function of the snr of the triggers in figure 2. It can be seen that, to a very good approximation, the errors fall into normal distributions<sup>1</sup> whose standard deviation is a monotonically decreasing function of the snr. Figure 3 shows

<sup>1</sup> We have also verified the Gaussianity of the distribution of errors in each population of the injections.

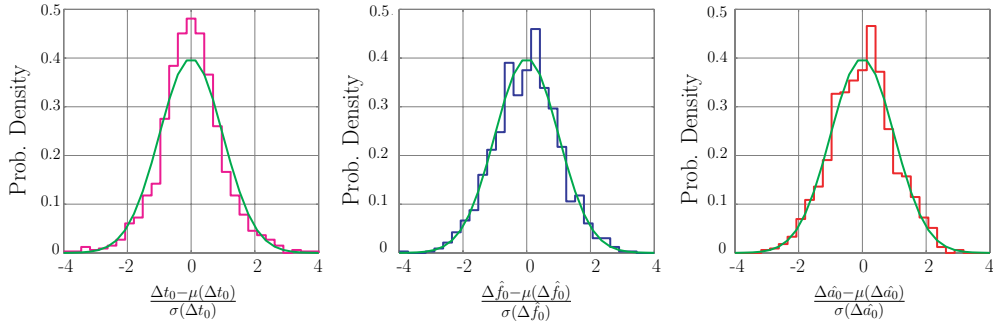


**Figure 1.** Distribution of the errors in estimating the central time, central frequency and RSS amplitude of the injected sine-Gaussian waveforms. The errors in the frequency and amplitude estimation are normalized by the injected value of the parameters, i.e.,  $\Delta\hat{f}_0 = \Delta f_0 / f_{\text{cen}}$  and  $\Delta\hat{a} = \Delta a / h_{\text{rss}}$ . Injections are done with nine different values of  $h_{\text{rss}}$  such that the snr of the injections ranges from  $\simeq 5$  to  $\simeq 300$  (see figure 2). Sample mean and standard deviation of each of the nine populations are estimated separately. Each error is converted into a reduced normal variable by subtracting the corresponding sample mean and by normalizing by the corresponding standard deviation. Also plotted are the probability densities of the standard normal distributions.

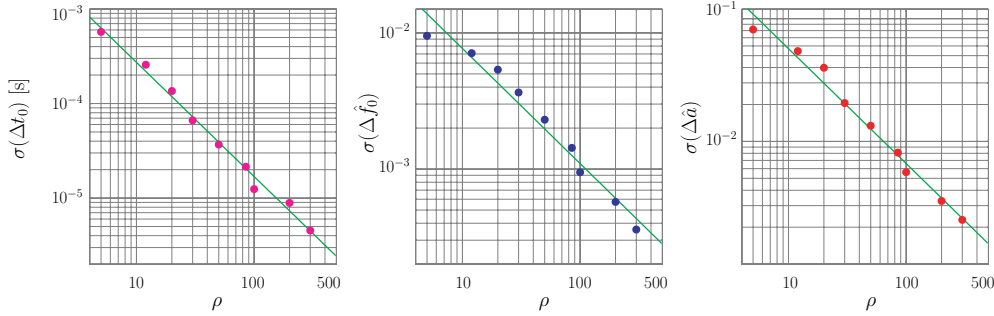


**Figure 2.** Standard deviation of the distribution of the errors (fractional errors in the case of  $f_0$  and  $a$ ) in estimating the parameters of the injected sine-Gaussian waveforms, plotted as a function of the snr of the triggers. Also shown are power-law fits to the data.

the mean errors in the parameter estimation which are indications of the systematic biases in the parameter estimation. The left panel shows a small bias in the estimation of  $t_0$ . But this is smaller, even, than the sampling period of the data used in the simulations ( $\simeq 61 \mu\text{s}$ ) and can be safely ignored.

### 3. The standard statistical veto

All currently operating GW detectors face the problem that several instrumental and environmental noises can couple to the GW channel. Therefore, it is desirable to identify, in the GW data stream, those events which can be shown to have a local instrumental or environmental source, and exclude them from any astrophysical analysis.

At each GW detector a multitude of sensors is installed to monitor instrumental noise sources (for instance, laser power noise) and environmental noise sources (such as magnetic fields). In the following, we will refer to both instrumental and environmental noises as technical noise sources.

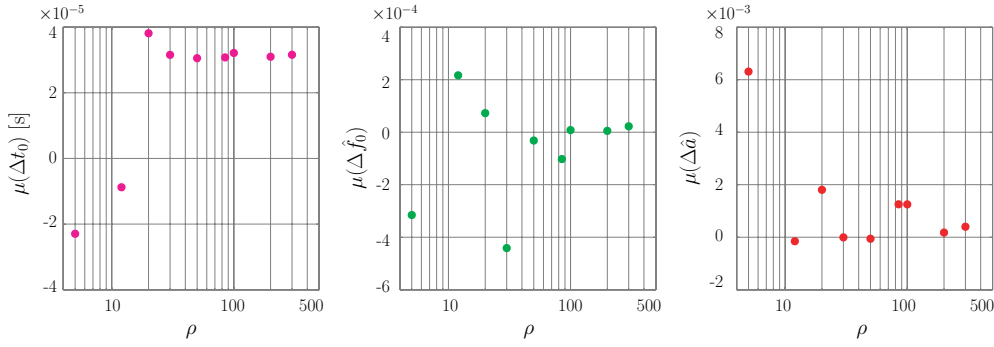


**Figure 3.** Mean errors (fractional errors in the case of  $f_0$  and  $a$ ) in the parameter estimation, plotted as a function of the snr of the triggers.

If the detected events in the GW channel are caused by a technical noise source, there will be a significant statistical correlation between the events of the GW channel and those detected in the recording of any device which monitors the noise source. Indeed, this assumes that both the main detector output and the auxiliary channel are properly recorded, and that the detection algorithm does a good job of detecting and parameterizing any glitch events in the data streams. Even in the case when the coupling mechanism from the technical noise source to GW channel cannot be measured, we can use the statistical correlation to veto the coincident events.

In order that we end up with a sufficiently low false-veto rate, we must restrict ourselves (for the time being) to auxiliary channels which can contain no GW information.

### 3.1. The method in general

Usually a simple statistical veto is based on the comparison of the time,  $t_0^H$ , of the event in the GW channel and the time,  $t_0^X$ , of the event in an auxiliary channel. Two events,  $H[i]$  and  $X[j]$ , are defined as being coincident when they are separated in time by less than a chosen time window,  $t_{\text{win}}$ :

$$|t_0^H[i] - t_0^X[j]| < t_{\text{win}}. \quad (12)$$

Every event,  $H[i]$ , that is time coincident with at least one event from the auxiliary channel is vetoed.

The performance of a veto depends on many parameters (such as the event rates in the individual channels) and needs to be evaluated in order to best tune the coincidence windows used; this is typically an iterative process. The following measures can be useful to judge the performance of a veto:

- The *efficiency*,  $E_X$ , is the percentage of triggers in the GW channel that are vetoed by the use of the events from the auxiliary channel,  $X$ .
- The *background*,  $B_X$ , is the percentage/rate of triggers in the GW channel that are *accidentally* vetoed by the use of the events of the auxiliary channel,  $X$ . In general there are two possible classes of coincident events:
  - (i) The event  $H[i]$  is either caused by or originates from the same source as the event  $X[j]$ .
  - (ii) The event  $H[i]$  is not caused by any event recorded in the auxiliary channel, but by accident there happens to be an independent event  $X[j]$  that is time coincident with the event  $H[i]$ .

By time-shifting the events in the GW channel with respect to the events in the auxiliary channel, it is possible to destroy the causal relationship between the correlated events of the two channels and by that to determine the background (or accidental) rate.

- The *significance*,  $S_X$ , is defined as the ratio of efficiency and background and can be seen as the main figure of merit of a veto analysis. This can be illustrated by some examples. A veto that has a high efficiency of 50% might also have a high background of, for example, 5%, which would mean that we would falsely veto a large number of potential GW signals. On the other hand, a very low background of 0.01% does not necessarily guarantee a good veto performance, as it can still have a low efficiency of, say, 0.03%. That is why we choose here the ratio of efficiency and background as another good way of judging the trade-off between the efficiency and the background. When changing the width of a coincidence window, both the efficiency and the background are changed as well, but in general with different slopes.
- The *use-percentage*,  $U_X$ , is another means of the measuring the veto performance. It is defined as the percentage of the events in the auxiliary channel that can veto an event in the GW channel.

*3.1.1. Additional coincident windows.* In order to improve the significance of a veto, it might be useful to demand that not only are two events coincident in time, but also that other parameters of the events are taken into account. If the event,  $X[j]$ , is the origin of the event  $H[i]$ , for instance, then the central frequency of the two events or their duration might also show a correlation. Of course, the strength of the correlation depends strongly on the coupling from channel  $X$  to the GW channel,  $H$ , and also on the noise level and the stationarity of the noise in the two channels. In the worst case, the correlation might be completely destroyed. However, in GEO 600 we found some cases where the application of a second coincidence condition clearly improves the significance of a statistical veto.

In the following sections, we will also apply an additional coincidence window,  $f_{\text{win}}$ , for the central frequency of the events. In that case, an event,  $H[i]$ , in the GW channel is vetoed by the event,  $X[j]$ , from the auxiliary channel only when the following equations are fulfilled:

$$|t_0^H[i] - t_0^X[j]| < t_{\text{win}} \quad (13)$$

and

$$|f_0^H[i] - f_0^X[j]| < f_{\text{win}}, \quad (14)$$

where  $f_0^H[i]$  and  $f_0^X[j]$  are the central frequencies of the two events.

Ideally, the window chosen to test the consistency of the central frequencies of the two events should be determined separately for each pair of coincident triggers since the bias in the estimation of the central frequencies depends on the waveform and snr of signal as it is detected in each channel.

### *3.2. Application of a standard statistical veto GEO S5 data*

In this section, we will show some investigations done in order to find out whether it is reasonable to use a monitor of the main site power supply (mains) as a veto channel. Glitches in the mains can potentially couple in various ways to the GW channel. A glitch in the mains causes a glitch in the magnetic field surrounding the power line which can then interact with magnets glued onto the mirror [24]. Or the magnetic glitch can directly induce a voltage glitch in a piece of electronics used for control or readout of the detector. On the other hand, it is highly unlikely that a GW could couple back to the mains monitor.

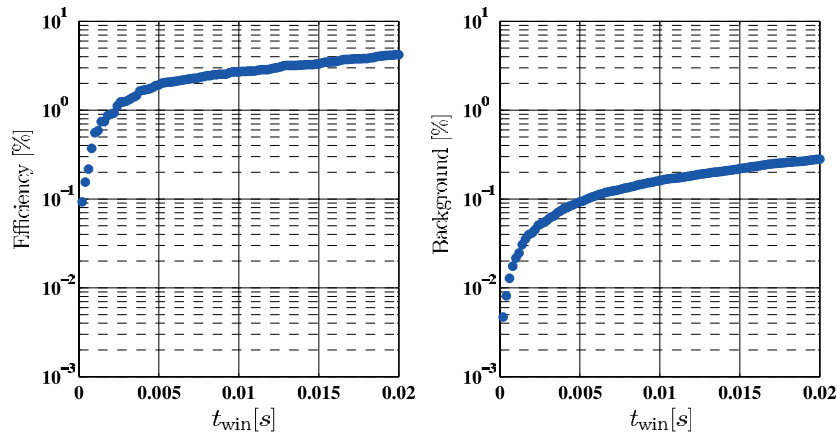


**Figure 4.** Exemplary application of a statistical veto to a 24 h stretch of GEO data using a GW-free channel (in this case a mains monitor) as veto channel. The efficiency and background are given as a function of the size of the coincidence time window. The data set used consisted of 3228 and 7725 events in the GW channel and the mains monitor, respectively.

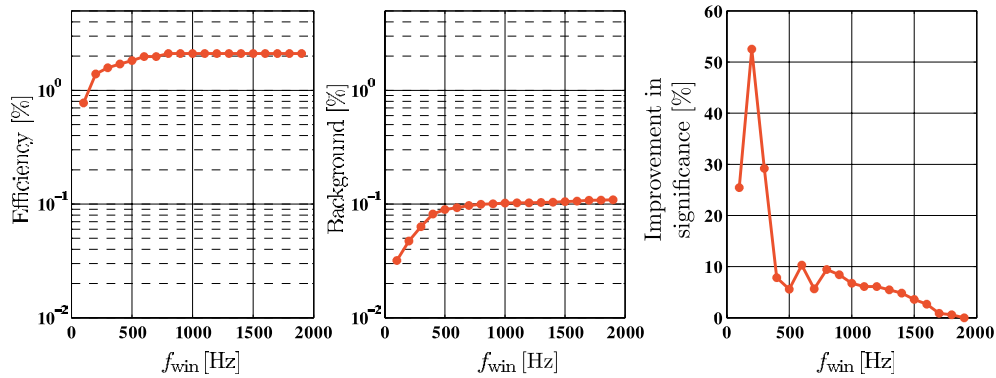


**Figure 5.** Exemplary application of a statistical veto including an additional coincidence condition for the central frequency of the events. The same data set as for figure 4 is used. A time coincidence window of 6 ms is applied. The background and efficiency are plotted versus the size of the coincidence window for the central frequency. In addition, the right-hand plot shows the improvement in significance versus the size of the frequency window. The improvement of significance is normalized to the case where no frequency coincidence window is applied.

Figure 4 shows the application of a standard statistical veto to the GW channel using a mains monitor as veto channel. The efficiency and background rate are plotted for time windows between 0 and 20 ms. The shapes of both curves are roughly the same, i.e., the significance stays roughly constant around a value of 20 for different sizes of the time coincidence window.

If we choose a time window of 6 ms in order to get a background of 0.1%, we achieve an efficiency of about 2%. Figure 5 shows (for the same set of data and a fixed time window of 6 ms) the effect of including an additional coincidence window for the central frequency of the events.

The right-hand plot of figure 5 shows the improvement in the significance for different sizes of the frequency coincidence window, compared to the case where only a coincidence

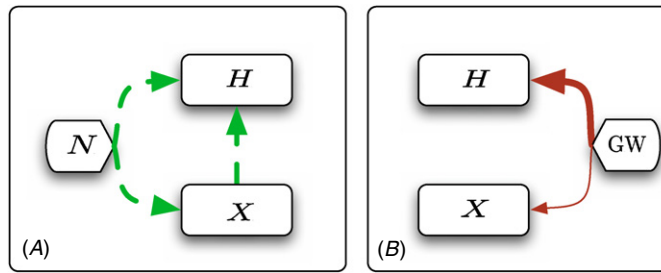


**Figure 6.** A schematic view of two different scenarios in which coincident transient events can appear in both the main GW channel,  $H$ , and an auxiliary channel,  $X$ . The first (panel  $A$ ) shows coincident events arising from a single noise source,  $N$ , which couples events to  $H$  either directly or via subsystem  $X$  or both. The second scenario (panel  $B$ ) shows the case where gravitational waves also couple to the auxiliary channel directly. (Obviously, the auxiliary channel is less sensitive to GWs than the main detector output, otherwise it would be used as the main GW channel.)

window for time of the events is applied. In this case, for all sizes of the frequency coincidence window, the significance is improved. A maximal improvement of about 50% is achieved for a frequency window of 200 Hz.

If we choose windows,  $t_{\text{win}} = 6$  ms and  $f_{\text{win}} = 200$  Hz, we get an efficiency of 1.5%, a background of 0.05%, a use-percentage of 0.6% and a significance of 30.

This example demonstrates the usefulness of additional coincidence windows.

#### 4. A statistical veto for channels containing GW information

In the previous section, we described the statistical veto method using an auxiliary channel containing no GW information. In this section, we will show that, under certain conditions, and when handled with care, a reliable statistical veto can also be based on a veto channel which can contain GW information.

Figure 6 shows two scenarios. Panel  $A$ ) describes the case where there is an (unknown) coupling of a noise source,  $N$ , into both the main GW channel and an auxiliary channel,  $X$ ; for this case, the standard statistical veto described in section 3 can be applied. Panel  $B$ ) illustrates the case where the auxiliary channel is also sensitive (but to a lesser degree) to GWs. In order to apply a statistical veto (with a sufficiently low false-veto rate), to situations that potentially include couplings as depicted in panel  $B$ ), we have to introduce further coincidence conditions, such as a frequency-dependent amplitude cut. The application of this method requires a rough knowledge of the (complicated) frequency-dependent sensitivity ratio of the auxiliary channel compared to the  $H$  channel. Note that this sensitivity ratio will, in general, be a complicated function of frequency and time. For the remainder of this paper this sensitivity ratio is denoted by  $\alpha$ .

##### 4.1. The method in general

In the presence of a coupling from GW signals to the veto channel, we will have two classes of coincidence events to consider when applying a standard statistical veto:

- Noise events that couple via the (green) dashed lines of figure 6. These are the events we would like to veto.
- GW-like events that appear in the veto channel directly.

It is essential to discriminate these two populations and exclude events from the latter class from being vetoed.

A possible way to proceed with such potential veto channels is to compare the amplitudes  $a^H[i]$  and  $a^X[j]$  of the two coincident triggers  $H[i]$  and  $X[j]$ . In the case that the event  $X[j]$  arises directly from the GW-like event,  $H[i]$ , the following (ideal) relation should hold:

$$\frac{a^X[j]}{a^H[i]} = |\alpha(f_0^H[i])|, \quad (15)$$

where  $|\alpha(f_0^H[i])|$  is the magnitude of the sensitivity ratio of the auxiliary channel compared to the  $H$  channel evaluated at the central frequency of the event,  $H[i]$ , in the GW channel.

If all quantities in equation (15) are known, the application of the statistical veto is rather simple. First of all, the coincident events need to be determined in the same way as for the standard statistical veto. Secondly, for each pair of events, the ratio of the two amplitudes is compared. If this ratio equals the magnitude of the known sensitivity ratio at the central frequency of the event, the event in the GW channel is not vetoed. If the amplitude ratio is not consistent with  $\alpha$ , the event  $H[i]$  is vetoed.

It is also possible that more than one event in the veto channel is coincident with the event  $H[i]$ . In this case, the  $H$  event is excluded from being vetoed if at least one of the coincident pairs satisfies equation (15).

#### 4.2. A 'real-world' scenario

In reality, equation (15) needs to be extended to account for several systematic and statistical errors. Probably the largest contribution to the error originates from the amplitude estimation of the burst events. The errors associated with the amplitude estimation of the events  $H[i]$  and  $X[j]$  are referred to as  $\Delta a^H[i]$  and  $\Delta a^X[j]$ , respectively. Also, the measurement of the sensitivity ratio,  $\alpha$ , can be a source of error. Moreover,  $\alpha$  can also be non-stationary over time. We represent the cumulative errors due to these two effects by  $\epsilon$ .

Considering these errors, we make a simple generalization of equation (15) into the 'real-life' situation. In order to veto an event,  $H[i]$ , in the GW channel, we first require that it is coincident with another event,  $X[j]$ , in the veto channel in the sense of a standard statistical veto (in time and frequency), and secondly that it satisfies either of the following conditions:

$$\frac{a^X[j]}{a^H[i]} < \frac{|\alpha(f_0^H[i])|}{(1 + \epsilon)}, \quad (16)$$

or

$$\frac{a^X[j]}{a^H[i]} > |\alpha(f_0^H[i])|(1 + \epsilon). \quad (17)$$

We will call the veto method, based on the condition described above, a *frequency-dependent amplitude cut*, because we cut the events with a certain amplitude ratio out of the list of coincident vetoed events.

### 5. Application of a statistical veto with an amplitude consistency check to GEO 600 data

In May 2006, a significant increase in the glitch rate of the main GW channel ( $H$ ) of GEO 600 was observed. A broken air conditioning system blew unfiltered air into the main clean room and increased the dust particle concentration by more than one order of magnitude. It turned out that the increase in the glitch rate of  $H$  originated from dust particles falling through the main output beam of the interferometer. Many glitches in the recorded dc light power hitting

the main photodiode (referred to as  $\mathcal{P}_{\text{dc}}$ ) were observed to be coincident with glitches in  $H$ . However, tests involving injecting different signals (noise, sinusoidal, burst events) into the differential length control actuator for the Michelson interferometer (to mimic the effect of a GW) showed that  $\mathcal{P}_{\text{dc}}$  can contain, to a non-negligible degree, some GW signal. Hence, using a standard statistical veto could, undesirably, also veto many potential GW events.

In the following three subsections, we will present the results of applying a statistical veto with an amplitude consistency check to GEO 600 data using  $\mathcal{P}_{\text{dc}}$  as the veto channel. Two different periods of time are analysed. The analysis of a long stretch of data covering the entire month of September 2006 (where the dust concentration in the clean room was nominal) is presented in subsection 5.1. An 8 h stretch of science data from May 2006 (where a high dust concentration in the clean room was observed) is analysed in subsection 5.2. There are only short data stretches available for this period because the broken air conditioning system was fixed within a few days. However, even with the nominal dust concentration restored, still, dust glitches contribute to the glitch rate of  $H$ . Finally, the performance of the veto for both periods is compared in subsection 5.3.

### 5.1. Data set 1: full September 2006 with low dust concentration

For both data sets, and the hardware injections, firstly a coincidence analysis is performed using a time coincidence window of 8 ms and a frequency coincidence window of 1 kHz.<sup>2</sup> The upper plot of figure 7 shows the ratio of the amplitude of the coincident events from  $\mathcal{P}_{\text{dc}}$  and  $H$  versus the central frequency of the event in  $H$ . The (blue) diamonds, corresponding to the GW-like hardware injections, are close to the measured sensitivity ratio,  $\alpha$  (as expected); all the coincident events from the first data set (represented by the purple points) show either a similar amplitude ratio or a higher one. If the ratio is similar to the hardware injections, the points most probably correspond to GW-like events. If the amplitude ratio is higher, this means that  $\mathcal{P}_{\text{dc}}$  events show a higher amplitude than is consistent with events originating from direct coupling. As we do not observe any pairs of events with an amplitude ratio much lower than from the hardware injections, it is reasonable to simplify equation (17) to the single condition,

$$\frac{a^X[j]}{a^H[i]} > |\alpha(f_0^H[i])|(1 + \epsilon). \quad (18)$$

Over one month,  $\alpha$  was measured a few times<sup>3</sup> and the fluctuations were observed to be less than 50%. The main error contribution of the amplitude estimation of the events can be described by three times the standard deviation ( $3\sigma$ ) given in the right-hand plot of figure 2. The lowest snr of an event contained in this analysis is about 4, which means that the maximum error in estimating the amplitude of sine-Gaussian waveforms in Gaussian noise is about 50% (see figure 2). Motivated from these observations, we empirically allow an error  $\epsilon = 2$ . However, there might be a better way to choose  $\epsilon$ , for example, by doing many hardware injections using a wide morphology of waveforms, which we leave as future work.

In the end we get the final set of three veto conditions:

$$|t_0^X[j] - t_0^H[i]| < 8 \text{ ms}, \quad (19)$$

$$|f_0^X[j] - f_0^H[i]| < 1 \text{ kHz}, \quad (20)$$

<sup>2</sup> These window sizes are chosen (from efficiency and background maps) to give the best efficiency for an acceptable (less than one per day) background rate.

<sup>3</sup> The sensitivity ratio is measured by injecting white noise into the Michelson length control actuators so as to dominate the noise in  $H$  and  $\mathcal{P}_{\text{dc}}$ . The ratio of the noise in  $H$  and  $\mathcal{P}_{\text{dc}}$  can then be computed.

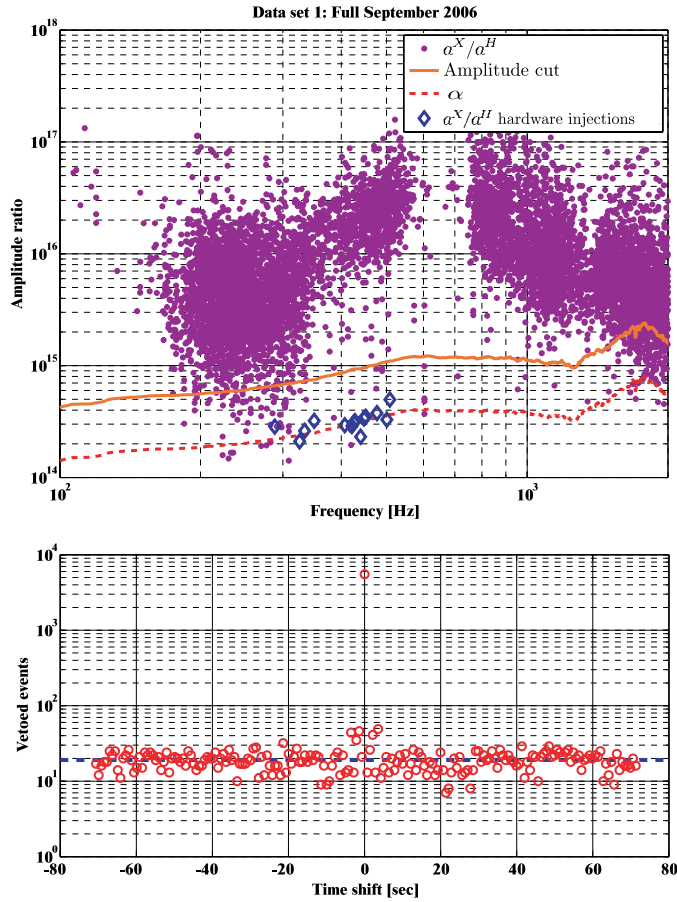


**Figure 7.** Upper plot: application of a statistical veto with an amplitude consistency check to GEO 600 data for the entire month of September 2006. The (red) dashed line is a measurement of the sensitivity ratio,  $\alpha$ . The (blue) diamonds are the amplitude ratios of the coincident events in  $\mathcal{P}_{dc}$  and  $H$  from GW-like burst hardware injections. The hardware injections are consistent with  $\alpha$ . The solid (orange) line is the chosen amplitude cut, corresponding to  $\epsilon = 2$ . The (purple) points indicate the amplitude ratio of the coincident events from  $\mathcal{P}_{dc}$  and  $H$  for the entire month of September. Each  $H$  event corresponding to a point above the solid line is vetoed, while each point below the solid line is taken as being consistent with a GW signal and is not vetoed. Lower plot: a time-shift analysis of the statistical veto with an amplitude consistency check for data set 1. 5517 events in  $H$  are vetoed, while the background of accidentally vetoed events amounts to 19.1 events per month. Note: the two apparent populations (below and above 600 Hz) are only an artefact of the analysis. At these frequencies, the violin modes of the main test-mass suspensions ‘blind’ the mHACR algorithm such that no events are detected.

and

$$\frac{a^X[j]}{a^H[i]} > 3|\alpha(f_0^H[i])|. \quad (21)$$

The last condition can be seen as an amplitude cut. The solid (orange) line in figure 7 indicates the level of this amplitude cut. Each  $H$  event corresponding to a (purple) point above the solid line is vetoed, while each point below the solid line is taken as being consistent with a potential GW signal and is not vetoed. By introducing the amplitude cut the veto efficiency

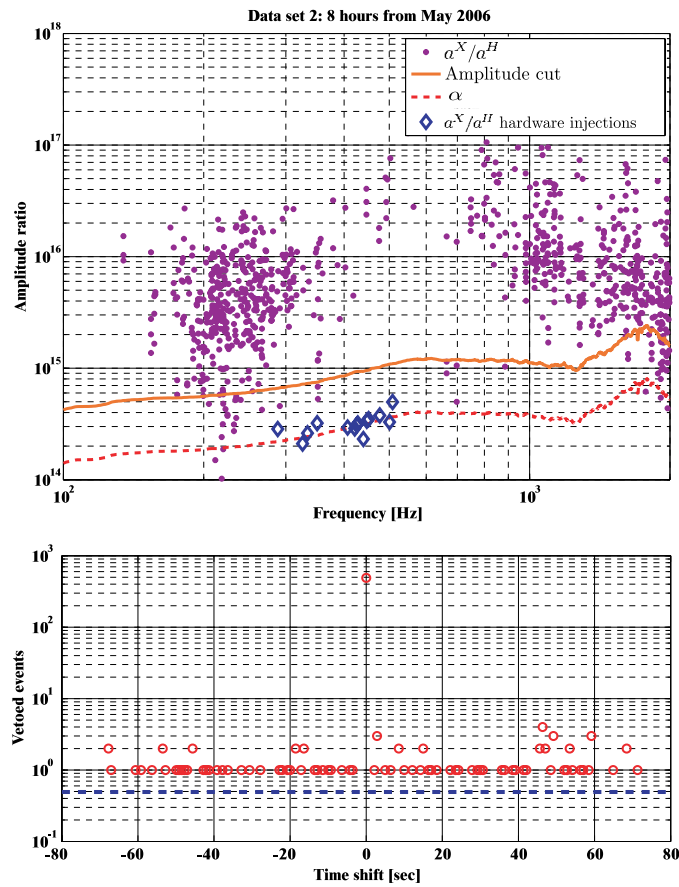


**Figure 8.** Upper plot: the application of a statistical veto with an amplitude consistency check to 8 h of GEO data from May. For further details, see figure 7. Lower plot: a time-shift analysis of the statistical veto with an amplitude consistency check for data set 2. 291 events in  $H$  are vetoed, while the background of accidentally vetoed events amounts to 0.49 events per 8 h.

is reduced from 5.94 to 5.72%. The background rate of this veto is estimated by time-shifting the  $H$  events and is indicated by the (blue) dashed line in the lower plot of figure 7.

### 5.2. Data set 2: 8 h from May 2006 with high dust concentration

Data set 2 is from a time with a high dust concentration in the main clean room. For the analysis, identical veto conditions are applied as for data set 1. The result of the veto application is shown in figure 8.

For this set of data, a high veto efficiency of greater than 20% is obtained. The background rate of this veto, estimated from a time-shift analysis, is indicated by the (blue) dashed line in the lower subplot of figure 8.

### 5.3. Performance summary of the veto analysis

The results of applying a statistical veto based on  $\mathcal{P}_{dc}$ , together with an amplitude consistency check, are summarized in table 2.

**Table 2.** A summary of the results of applying a statistical veto with an amplitude consistency check to two different data sets from GEO 600.

Data set	1	2
Total number of events in $H$	96 454	2281
Total number of events in $\mathcal{P}_{dc}$	26 600	615
Event rate in $H$ ( $\text{h}^{-1}$ )	134	285
Event rate in $\mathcal{P}_{dc}$ ( $\text{h}^{-1}$ )	37	77
Number of events vetoed	5517	491
Efficiency (%)	5.72	21.5
Background (%)	0.02	0.02
Significance	286	1075
Use-percentage (%)	20.7	79.8

As we can see, the use-percentage has changed between the two data sets. This change arises from the fact that the glitches detected in  $\mathcal{P}_{dc}$  are drawn from many different populations. This signal is not only sensitive to dust particles falling through the beam, but also to any other power fluctuations of the beam, for example, amplitude noise of the laser.

## 6. Summary

We showed that the performance of a standard statistical veto can be improved by application of more than one coincidence window. Furthermore, a new veto method was developed which allows the use of veto channels which can contain GW signals originating either from back-coupling or from a direct coupling. By introducing an amplitude consistency check, safe statistical vetoes can be derived from interferometer channels. GW-like hardware injections have been performed to demonstrate the robustness of this veto method. Application of a statistical veto with an amplitude consistency check to data from the GEO 600 detector was shown to perform well, giving a veto efficiency of up to 20% and a use-percentage of up to 80%. This new method is generally applicable and can also be used on the data from other GW detectors.

## Acknowledgments

The authors are grateful for support from PPARC and the University of Glasgow in the UK, and the BMBF and the state of Lower Saxony in Germany. This document has been assigned LIGO Laboratory document number LIGO-P060058-00-Z.

## References

- [1] Hild S (for the LIGO Scientific Collaboration) 2006 The status of GEO 600 *Class. Quantum Grav.* **23** S643–51
- [2] Waldman S J (for the LIGO Science Collaboration) 2006 Status of LIGO at the start of the fifth science run *Class. Quantum Grav.* **23** S653–60
- [3] Acernese F *et al* 2006 The Virgo status *Class. Quantum Grav.* **23** S635–42
- [4] Ando M and The TAMA Collaboration 2005 Current status of the TAMA300 gravitational-wave detector *Class. Quantum Grav.* **22** S881–9
- [5] Ajith P, Hewitson M, Smith J R and Strain K A 2006 Robust vetoes for gravitational-wave burst triggers using known instrumental couplings *Class. Quantum Grav.* **23** S825–37
- [6] Hanna C R (for the LIGO Scientific Collaboration) 2006 Reducing gravitational wave false alarms using signals at the antisymmetric port in LIGO detectors *Class. Quantum Grav.* **23** S17–22

- [7] Kötter K, Heng I S, Hewitson M, Strain K A, Woan G and Ward H 2003 PQMon: a powerful veto for burst events *Class. Quantum Grav.* **20** S895–902
- [8] Hewitson M and Ajith P 2005 Using the null-stream of GEO 600 to veto transient events in the detector output *Class. Quantum Grav.* **22** 4903–12
- [9] Di Credico A (for the LIGO Scientific Collaboration) 2005 Gravitational wave burst vetoes in the LIGO S2 and S3 data analyses *Class. Quantum Grav.* **22** S1051–8
- [10] Akutsu T, Ando M, Kanda N, Tatsumi D, Telada S, Miyoki S and Ohashi M and The TAMA Collaboration 2006 Veto analysis for gravitational wave burst signals in TAMA300 data using an ALF filter *Class. Quantum Grav.* **23** S23–8
- [11] Beauville F *et al* (The Joint LIGO/Virgo Working Group) 2005 A first comparison of search methods for gravitational wave bursts using LIGO and Virgo simulated data *Class. Quantum Grav.* **22** S1293–301
- [12] Ajith P, Hewitson M and Heng I S 2006 Null-stream veto for two co-located detectors: implementation issues *Class. Quantum Grav.* **23** S741–9
- [13] Wen L and Schutz B F 2005 Coherent network detection of gravitational waves: the redundancy veto *Class. Quantum Grav.* **22** S1321–35
- [14] Cadonati L 2004 Coherent waveform consistency test for LIGO burst candidates *Class. Quantum Grav.* **21** S1695–703
- [15] Rakhmanov M and Klimentko S 2005 A cross-correlation method for burst searches with networks of misaligned gravitational-wave detectors *Class. Quantum Grav.* **22** S1311–20
- [16] Heng I S, Salemi F and Ortolan A 2003 Methods for multi-detector burst gravitational wave search *Class. Quantum Grav.* **20** S617–22
- [17] Balasubramanian R, Grote H, Heng I S, Hewitson M, Lück H, Smith J R, Strain K A, Ward H and Willke B 2005 Results from the first burst hardware injections performed on GEO 600 *Class. Quantum Grav.* **22** 3015–28
- [18] Heng I S, Balasubramanian R, Sathyaprakash B S and Schutz B F 2004 First steps towards characterizing the hierarchical algorithm for curves and ridges pipeline *Class. Quantum Grav.* **21** S821–6
- [19] Salvador R, Valeriano J, Pons X and Diaz-Delgado R 2000 A semi-automatic methodology to detect fire scars in shrubs and evergreen forests with Landsat MSS time series *Int. J. Remote Sensing* **21** 655–71
- [20] Fischer P, Helmich A, Lindner M, Wermes N and Blanquart L 2000 A photon counting pixel chip with energy windowing *IEEE Trans. Nucl. Sci.* **47** 881
- [21] Stuver A L and Finn L S 2006 A first comparison of SLOPE and other LIGO burst event trigger generators *Class. Quantum Grav.* **23** S733–40
- [22] Cadonati L and Márka S 2005 CorrPower: a cross-correlation-based algorithm for triggered and untriggered gravitational-wave burst searches *Class. Quantum Grav.* **22** S1159–67
- [23] Clapson A-C, Barsuglia M, Bizouard M-A, Brisson V, Cavalier F, Davier M, Hello P, Kreckelberg S and Varvella M 2005 A gravitational wave burst search method based on the S transform *Class. Quantum Grav.* **22** S1381–90
- [24] Gossler S *et al* 2002 The modecleaner system and suspension aspects of GEO 600 *Class. Quantum Grav.* **19** 1835–42